Investigation of hypersonic flow in the vki h3 wind tunnel: From facility characterization to boundary-layer interaction over low-temperature ablators

Investigation of hypersonic flow in the VKI H3 wind tunnel: from facility characterization to boundary-layer interaction over low-temperature ablators

P. W. Agostinelli*
Politecnico di Milano, Milan, 20133, Italy

A. Turchi†, D. Le Quang‡ and D. Masutti§
von Karman Institute for Fluid Dynamics, Sint-Genesius-Rode, 1640,Belgium

L. Vigevano¶
Politecnico di Milano, Milan, 20133, Italy

D. D'Ambrosio‖
Politecnico di Torino, Turin, 10129, Italy

O. Chazot**
von Karman Institute for Fluid Dynamics, Sint-Genesius-Rode, 1640,Belgium

This work deals with the characterization, in terms of operating conditions, of the H3 hypersonic wind tunnel of the von Karman Institute for Fluid Dynamics (VKI), thus providing a detailed and structured benchmark for the evaluation of testing capabilities in hypersonic wind tunnels, and with the experimental study of the interaction between the boundary layer and the ablation process of low temperature ablative materials. The flow characteristics of the test section of the H3 WT have been assessed by using a pitot rake, for a wider range of operating conditions with respect to previous calibrations. A CFD analysis of the diffuser-ejector system has been carried out to assess its performance, and an experimental test campaign has been performed in order to validate the CFD analyses and completely characterize the facility operating conditions. Finally, a series of experiments with models of increasing size and different shapes has been carried out to determine the blockage effect in the tunnel test section. The H3 WT is then employed to study the boundary layer interaction with the ablative process on low temperature ablative models. These models have been built after having appropriately designed the sintering system. The Planar Laser Induced Fluorescence method has been applied to visualize the flow behavior: a laminar-turbulent transition due to the ablation process has been observed, together with the main flow structures.

I. Introduction

Since the first hypersonic vehicles were conceived, knowledge and interest in hypersonic flows have been increasing day after day, fostered by the use of hypersonic wind tunnels through which Aerospace Engineers can recreate the flow conditions encountered by these vehicles, for example during the re-entry phase into the atmosphere. Even nowadays, when new generation computers make it possible to simulate these flow conditions through very accurate Computational Fluid Dynamics analyses, experiments carried out in hypersonic wind tunnels remain essential to validate these codes and verify our design model [1]. In particular, the H3 hypersonic wind tunnel (WT) [2] of the von Karman Institute for Fluid Dynamics (VKI), has been widely used in the past decades, having a peak usage of up to 20 tests per day.

*Former MSc student, Dipartimento di Scienze e tecnologie aerospaziali, Via La Masa, 34. e-mail: walter-agostinelli@tiscali.it
†Senior Research Engineer, Aeronautics and Aerospace Department, Chaussée de Waterloo 72. AIAA Member.
‡Senior Research Engineer, Aeronautics and Aerospace Department, Chaussée de Waterloo 72.
§Former Senior Research Engineer, Aeronautics and Aerospace Department, Chaussée de Waterloo 72.
¶Professor, Dipartimento di Scienze e tecnologie aerospaziali, Via La Masa, 34. AIAA Member.
‖Professor, Dipartimento di Ingegneria Meccanica e Aerospaziale, Corso Duca degli Abruzzi, 24. AIAA Member.
**Professor and Head of Aeronautics and Aerospace Department, Chaussée de Waterloo 72. AIAA Member.

Presently, the H3 WT is being used for a European Space Agency project which aims to model the Phoebus re-entry capsule stability accounting for shape change due to material ablation [3]. This capsule, made by low temperature ablative material (i.e. naphthalene or camphor), has quite critical dimensions for the H3 facility test capability and led the tunnel to be operated at its limit conditions due to the blockage effect [4]. Many works in the past decades have underlined how the uncertainty source in experimental tests, that is usually neglected or at least overlooked, is the uncertainty in the flow conditions. It has been shown that the quality in measuring a drag coefficient for a certain model, for example, is mastered by the uncertainty in the flow conditions leaving to the uncertainty coming from instrumentation a marginal role [5]. The characterization of the free-stream disturbance environment of the H3 WT has been recently performed [6] while the determination of the Mach number has been performed by many authors during the past decades [6–9]. However, the limited number of total flow conditions investigated in previous calibrations, suggested to perform a new calibration of the facility: in hypersonic wind tunnels is indeed very important to perform a calibration over the full range of flow conditions since they influence boundary layers at the nozzle wall hence modifying the flow expansion [4]. Moreover, the diffuser operation is strongly influenced by total flow conditions that can change the diffuser pressure recovery and hence the test chamber pressure [10]. Therefore, the present work aims to a broad investigation and evaluation of the H3 hypersonic testing capabilities and to analyze how it would be possible to adapt its design to extend its operation range. The evaluation of the testing capabilities of H3 WT is carried out with the characterization of the flow in free stream conditions (i.e. calibration) and with a model inside the test chamber, and with the characterization of the supersonic diffuser – ejector system in terms of efficiency, pressure recovery and blockage effects. Finally, the experimental investigation of the boundary layer – ablation process interaction using the planar laser induced fluorescence method on naphthalene models shows to what extent is possible to study hypersonic flows behavior within this facility. The characterization of the H3 facility leads to important suggestions in order to improve its design to extend its operation range, thus providing a detailed and structured benchmark for the evaluation of testing capabilities in hypersonic wind tunnels. Moreover, the application to low temperature ablative materials laid the groundwork for extending the literature available on the study on the interaction between the ablation process and the boundary layer.

II. The VKI H3 hypersonic wind tunnel

The H3 facility is a blowdown hypersonic wind tunnel equipped with a 15 cm exit diameter axisymmetric contoured nozzle and is able to produce a Mach 6 free jet flow of almost 12 cm uniform test core diameter [6–9, 11, 12].

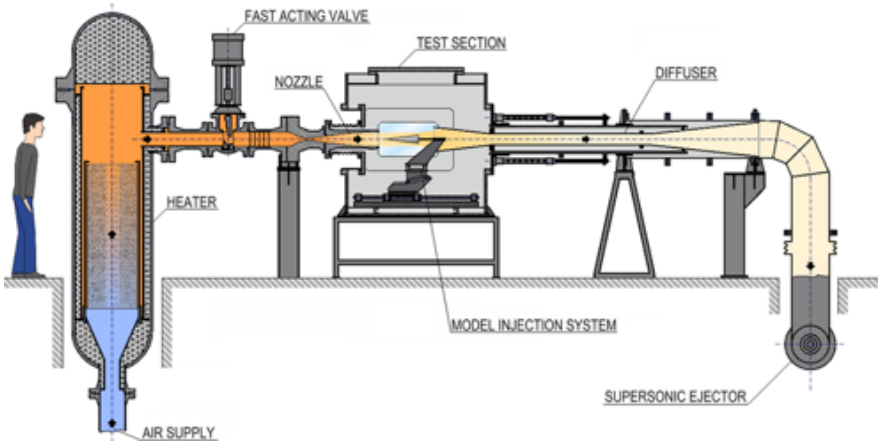

Fig. 1 Scheme of the H3 hypersonic wind tunnel

The operation and the structure of the H3 facility are the classical ones for blowdown facilities (Fig. 1). Test gas is air supplied from 40 bar air storage reservoirs at ambient temperature. To avoid condensation of the flow during the expansion in the nozzle, the supply air is heated in a storage heat exchanger prior to entering the tunnel settling chamber. The total pressure of the flow ranges from 6 to 35 bar and total temperature of the flow goes from 480 K to 550 K. Once the heater is heated up and the ejector has established a low pressure inside the test chamber, air is supplied through a fast activating valve. The flow accelerates to Mach 6 in the supersonic nozzle and is captured downstream the test chamber by a supersonic diffuser that provides the proper pressure recovery. To increase the flow momentum at the diffuser exit a supersonic ejector is used, discharging the flow into the atmosphere. The test section of the H-3 facility

is equipped with a three-degree-of-freedom traversing mechanism which provides for the electrically operated axial displacement of models and the variation of incidence and yaw angles. This mechanism is combined with a pneumatic system for the rapid injection of models into and out of the flow field: the usual procedure is to inject the model in the test chamber once the hypersonic flow has been established.

III. Facility characterization and calibration

A. Test chamber calibration

Calibrating a wind tunnel means to determine, throughout the range of total pressures and total temperatures allowed, the Mach number of the flow in the test chamber [4]. The Mach number is usually measured, for supersonic flows, by using a pitot pressure measurement (i.e. P_{02}) together with the total pressure measurement of the flow in the settling chamber (i.e. P_0) using Eq. 1.

$$\frac{P_{02}}{P_0} = \left[\frac{(\gamma+1)M^2}{(\gamma-1)M^2+2}\right]^{\frac{\gamma}{\gamma-1}} \left[\frac{\gamma+1}{2\gamma M^2-(\gamma-1)}\right]^{\frac{1}{\gamma-1}} \tag{1}$$

Since calibrating a wind tunnel is a quite expensive procedure, it is possible to use the so-called Modern Design of Experiments (DOE) in order to reduce the needed number of tests without affecting the data quality: for example, it is possible to create a response surface model that can predict, within a certain uncertainty, the average Mach number in the core flow for different flow total conditions [13, 14]. In the H3 case, even if only three variables are considered in the design space (P_0, T_0 and the axial position X), the required number of data points following the DOE becomes prohibitive. This difficulty was avoided by modifying continuously the pitot rake axial position during the test, thus obtaining a 2D map of the flow for each operating condition tested. In this way a regression model of the Mach number may be obtained as a function of total pressure and total temperature only.

1. Experimental setup

Different sensors were already installed in the H3 facility: the pressure transducer measuring the test chamber pressure at the wall, the one measuring the absolute flow total pressure and the type K thermocouple measuring the flow total temperature in the settling chamber just upstream the nozzle. Although these sensors give enough data to perform the major part of the experiments, they are not enough to completely characterize the H3 facility. In particular, in order to characterize the diffuser and ejector operation, it is needed to measure the total pressure of the ejector flow and the diffuser exit pressure. All the sensors have been calibrated before installation and a check of the previous sensors operation has been performed. In order to read the pitot rake pressures a miniature pressure scanner ESP 16HD (Pressure System) with 16 channels and a DAQ Pressure Scanner Acquisition System have been checked and calibrated. The pitot rake tubes are spanning 110 mm of core flow [9] and have an inner diameter of 0.5 mm: the Reynolds number based on tubes diameter in typical test conditions is of 10^4, that is well above the suggested limit of 10^3 for considering wall friction effect [4]. A camera has been used to perform a visual tracking of the pitot rake position. Data on pitot pressures and flow conditions are synchronized in order to have all the measurements expressed in terms of pitot position, so as to obtain a 2D map of the flow Mach number by moving the pitot rake along the test section axis during the wind tunnel test.

2. Experimental results

The operating envelope with the previous calibrations data points and the planned calibration envelope are shown in Fig. 2. For each data point the pitot rake has been moved during the test from a starting position of 5 mm to 100 mm downstream the nozzle exit.

In Fig. 3, typical results of the experimental Mach number contours for the 20 bar case at two different total temperatures are presented. The flow is quite symmetric and slightly under expanded in these conditions, since it is accelerating along the axis, with the Mach number value increasing from 5.87 to 6.05. The difference between the flow conditions at the two investigated T_0 values are slight: in the test with the higher Reynolds number (i.e. low T_0 value at fixed P_0), the flow seems to expand less than the test with the lower Reynolds (i.e. high T_0 value); in the latter condition, the Mach number distribution is more uniform in the vertical direction.

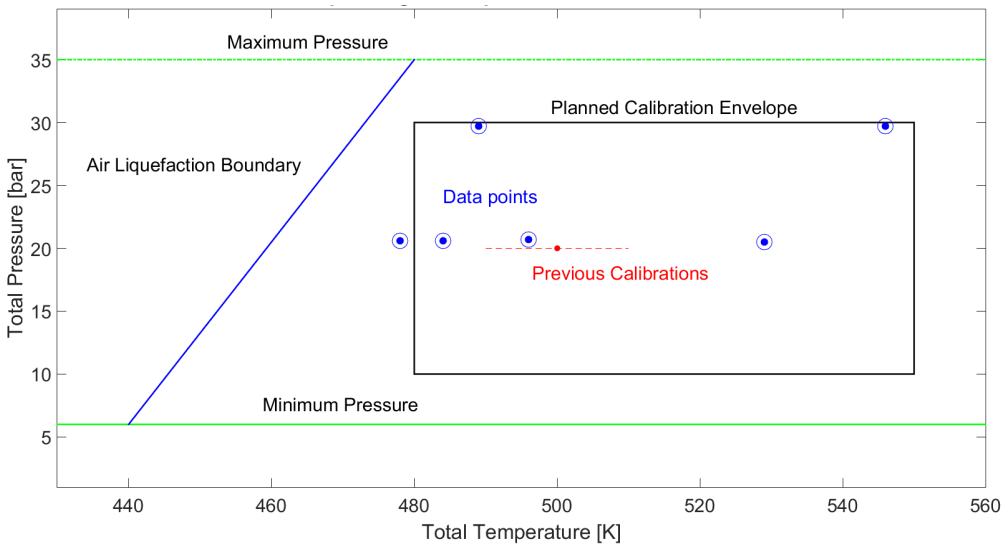

Fig. 2 Operating envelope for the VKI H3 hypersonic wind tunnel

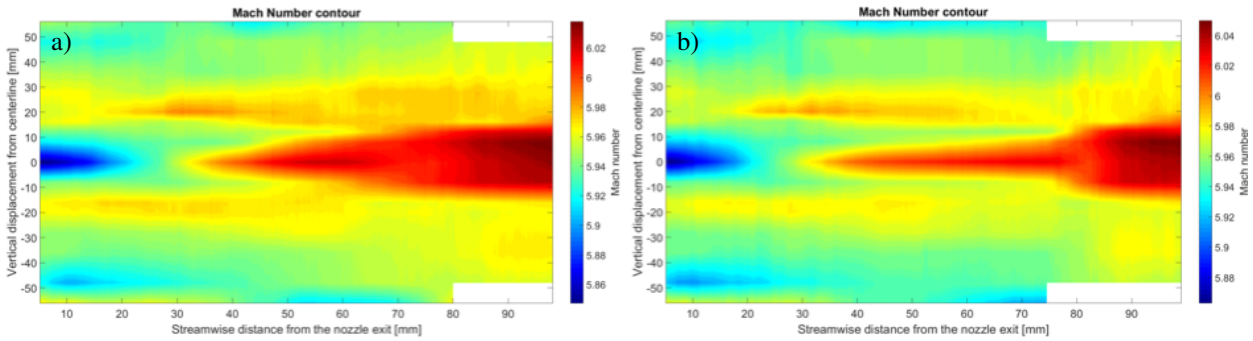

Fig. 3 Experimental Mach number contours for test with P_0 = 20.6 bar and T_0 = 478 K (a) and for test with P_0 = 20.5 bar and T_0 = 529 K (b)

Reynolds number only slightly affects the expansion of the flow leaving to the T0 value only a marginal role in determining the flow behavior in the test chamber. Moreover, for different total pressures P_0 (e.g. 20 and 30 bar) no large difference can be seen, except for a slight increase in the maximum Mach number with pressure. Important consideration regards the actual Mach number measured by the Pitot rake: the rake is indeed affecting the flow expansion in the test chamber due to the blockage effect. Therefore, the measured Mach values are significant only for tests carried out with models having blockage ratio comparable to the one of the pitot rake used. For a general characterization of the flow which is not linked to the particular blockage ratio used, it is more useful to look at the uniformity parameter, defined in Eq. 2 where M is the local Mach number and M_{avg} is the average value:

$$\gamma = 1 - \frac{|M - M_{avg}|}{M_{avg}} \tag{2}$$

Typical results for the uniformity parameter are shown in Fig. 4 for the 20 bar case (a) and 30 bar case (b). The maximum deviation from the mean is only the 2.2% and, as it is generally known in a supersonic flow, the non-uniformities concentrate along the axis. Models should be tested at a distance of 30 mm away from the axis in order to reduce flow non-uniformity.

A comparison of the measured Mach number vertical profiles with previous calibration data [6–9, 11] is presented in Fig. 5. The present data are very close to the ones taken by Kordulla [7] and are shifted downward if compared to Masutti [6] and Vanhèe [8] results, even if the shape and the symmetry of the curves are the same. The shift up of the

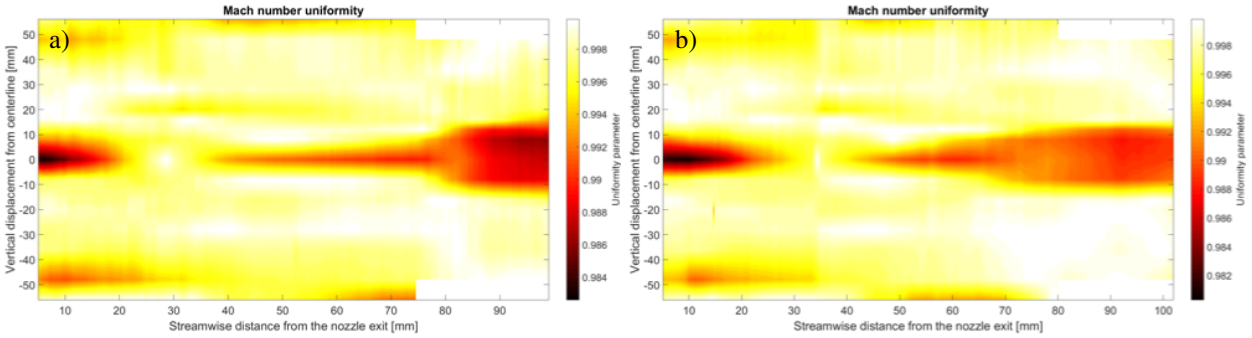

Fig. 4 Uniformity parameter contours for test with P_0 = 20.5 bar and T_0 = 529 K (a) and for test with P_0 = 29.7 bar and T_0 = 486 K (b)

measurements in [6] and [8] is due to the different free jet length and the pitot rake used. The free jet length affects diffuser efficiency and different models cause a different blockage effect and hence a different test chamber pressure (indeed Masutti and Vanhèe used a smaller Pitot rake).

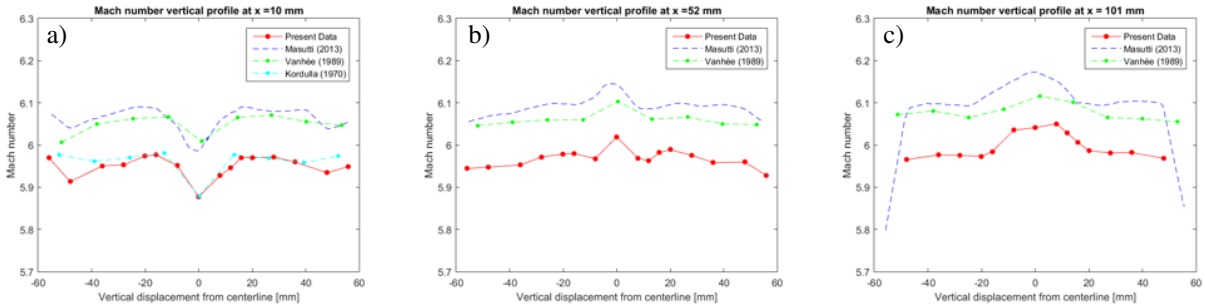

Fig. 5 Mach number vertical profiles comparison with previous calibrations at 10 (a), 52 (b) and 101 mm (c) from the nozzle exit

The comparison confirms the validity of the present data. A weak correlation has been found between the average Mach number in the test chamber and the flow total conditions: therefore, no response surface is believed to be needed for the analyzed operating envelope, that has an average Mach number of 5.97 for each investigated operating condition. Critical is instead the distance from the nozzle exit but, for this parameter, the actual response surface (i.e. the 2D map of the flow) for each flow condition has been measured.

B. Diffuser-ejector system

The two major aerodynamic components of the H3 facility are the supersonic diffuser and the supersonic ejector, which provides the necessary pressure ratio to start and run the tunnel. An open literature review [4, 10, 15–32] shows that the H3 diffuser-ejector geometry is in good agreement with the literature design rules and also with the geometric parameters of other two hypersonic tunnels, the SPES at the University of Naples Federico II [22] and the SCIROCCO at the Italian Aerospace Research Center (CIRA) [27]. Some concerns may be referred to the diffuser inlet and outlet geometry, that could be slightly improved: a better pressure recovery can be achieved by increasing the supersonic diffuser inlet diameter, to improve the capture of the flow deviated by large models, and decreasing the angle of the divergent part, in order to limit flow separation [25, 32].

1. CFD Analysis of the diffuser

Some CFD analyses of the H3 hypersonic diffuser have been carried out in order to verify its operation characteristics according to different boundary conditions, using the classical approach of Monti and Savino [22, 32]. The flow field in

the test chamber and in the diffuser has been numerically simulated with the ANSYS Fluent Software, solving the full Navier-Stokes equations for turbulent, compressible, axisymmetric flow, spatially discretized using a finite-volume scheme. The solver used is a density-based one, since it is more suitable for compressible flows. Numerical fluxes are calculated with the AUSM scheme [33]. The discretization used is second-order in space. Turbulence is modelled using the SST k-λ two-equation eddy-viscosity model [34]. The fluid has been modelled as a non polytropic ideal gas with specific heat at constant pressure c_p, viscosity μ and thermal conductivity λ varying as a piecewise-linear function of the temperature [35]. The gas chemical composition is kept constant since the total temperature of the fluid is not high enough to activate chemical reactions. The computational domain has the form of a cylindrical duct with variable cross-section that approximates the real test chamber and diffuser geometry (Fig. 6). The nozzle exit corresponds to the inlet of the computational domain while its outlet corresponds to the diffuser exit. The total pressure and temperature of the flow (which are assumed to be the same as in the settling chamber), together with the supersonic static pressure and the intensity and viscosity ratio for the turbulence modelling have been assigned as inlet boundary conditions. The conditions at the outlet have been assigned in terms of static pressure and back flow total temperature equal to 300 K. Diffuser and test chamber walls are modelled as stationary, with no slip conditions on smooth surfaces and constant temperature of 300 K. The domain geometry has been discretized using a structured mesh which has been refined in the regions near the diffuser walls. The mesh has been refined until a grid-independent solution is obtained.

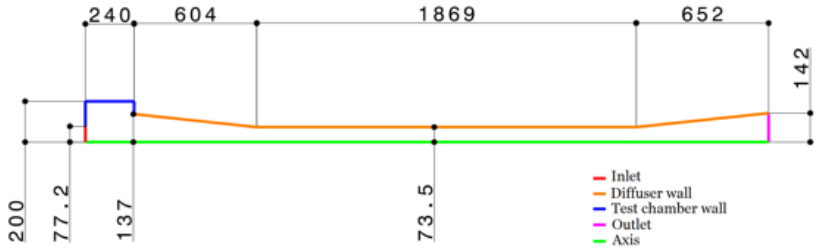

Fig. 6 Scheme of the computational domain for the H3 diffuser CFD analyses

The numerical simulations are initialized with a steady supersonic flow in the whole diffuser, obtained with a very small value of the static pressure at the diffuser exit (which corresponds to the physical starting of the tunnel). Once a converged solution has been obtained, the static pressure at the diffuser exit is increased step by step in order to find out for which maximum static pressure at the diffuser exit the diffuser itself is still able to maintain a low test chamber pressure with under-expanded conditions of the nozzle. This value corresponds to the maximum pressure recovery provided by the diffuser and gives us an idea about the diffuser operation characteristics and efficiency. One data point at the center of the H3 operating envelope has been chosen for the simulations (i.e. P_0 = 20 bar and T_0 = 500 K). The domain outlet pressure has been changed from 1 KPa, which corresponds to the pressure experimentally measured during the starting of the tunnel, to 60KPa for which under expanded flow conditions are no more present in the test chamber. In Fig. 7(a), we compare the Mach number along the axis for three different values of outlet pressure: 10 KPa, 30 KPa and 50 KPa. Simulations show that when the diffuser exit pressure is gradually increased, the corresponding pressure distribution along the diffuser changes. Increasing the pressure outlet, the subsonic region becomes longer and the shocks move upward from the diverging part (as in the case of 10 KPa) into the diffuser throat (i.e. 30 KPa and 50 KPa) without changing the flow upstream.

The different positions of the shocks influence the pressure recovery inside the diffuser: in the cases with low exit pressures, most of the recovery is allowed in the last part of the diffuser while, with high exit pressure, as the shockwave system is located in the central part, most of the recovery is located in the throat of the diffuser (Fig. 7(b)). The maximum value of the exit pressure, before the shockwaves enter in the test chamber, corresponds to the maximum pressure recovery that can be realized in the diffuser (in our case around 50 KPa), since by further increasing the diffuser exit pressure to 60KPa brings the flow into the test chamber to over-expanded conditions.

2. CFD Analysis of the diffuser-ejector system

The model used in these simulations is analogous to the one used in the previous diffuser analysis. The sketch of the considered domain (i.e. test chamber, main diffuser and ejector) is shown in Fig. 8. A second inlet, which corresponds to the ejector nozzle exit is located at the end of the main diffuser and introduces an additional mass flow rate in the domain.

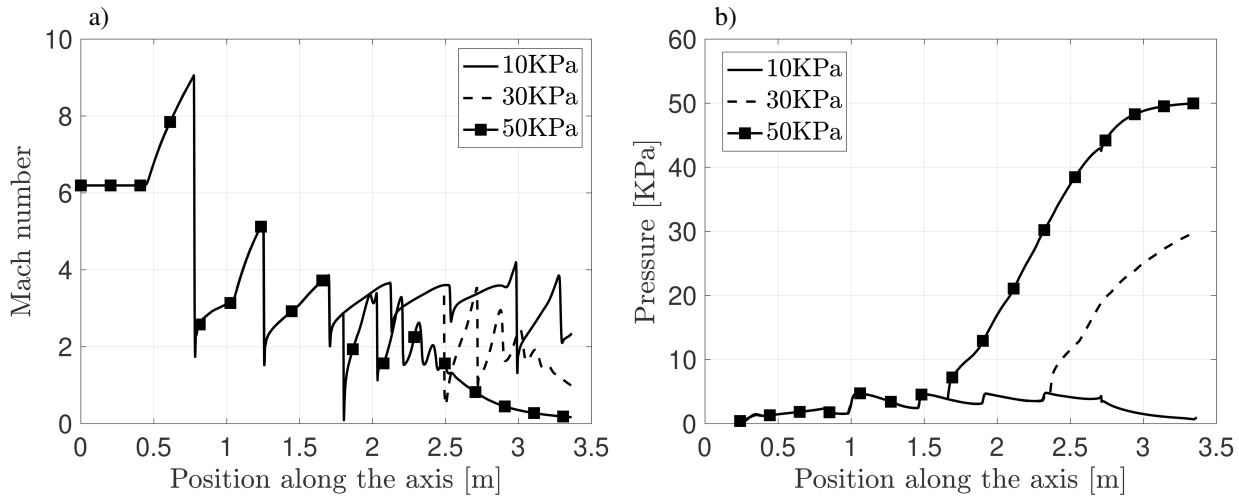

Fig. 7 Mach number along the H3 diffuser axis (a) and Static pressure at the wall (b), for P_{outlet} of 10 KPa, 30 KPa and 50 KPa

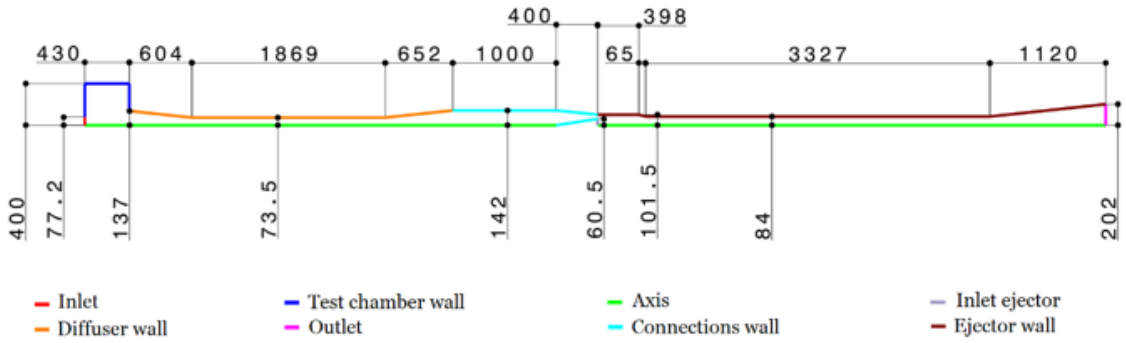

Fig. 8 Scheme of the computational domain for the H3 diffuser-ejector CFD analyses

We start the simulations with a very low pressure at the ejector exit and injecting air only through the second inlet (i.e. from the ejector nozzle): in this way a low pressure in the test chamber and in the main diffuser can be established by the ejector flow. The outlet pressure, after the starting procedure, has been set to 1 atm, since the ejector discharges into the atmosphere. At this point we "open" the facility fast activating valve at the operating conditions P_0 = 20 bar and T_0 = 500 K, in order to have a supersonic flow inside the whole facility. A range of ejector total pressure $P_{0,ej}$ between 25 and 10 bar (with $T_{0,ej}$ of 300 K), has been investigated in order to play with the different ejector regimes and find the value of $P_{0,ej}$ corresponding to the optimal ejector operation condition (Fig. 9).

From Fig. 9 it is evident that, by decreasing the ejector total pressure from 25 to 10 bar, no flow changes in the main diffuser can be seen. Indeed, when decreasing $P_{0,ej}$ the shocks in the ejector diffuser move upstream. At $P_{0,ej}$=10 bar the shocks have moved out of the ejector diffuser. This corresponds to a mixed regime, since there is a subsonic connection between the ejector exit and the main diffuser flow: the supersonic regime is no longer present in most of the ejector and the static pressure at the main diffuser exit increases if we further decrease $P_{0,ej}$. For $P_{0,ej}$=15 bar, instead, the supersonic regime is still present within the ejector. The transition point between supersonic and subsonic flow in the ejector is therefore obtained for 10 < $P_{0,ej}$ < 15 bar, a range confirmed by the experiments. To validate these analyses, it is also interesting to notice that the static pressure computed at the main diffuser exit due to the ejector operation is of 45 KPa, which is below the maximum value found with our previous analyses (i.e. 50 KPa) and which corresponds to the experimental measured value.

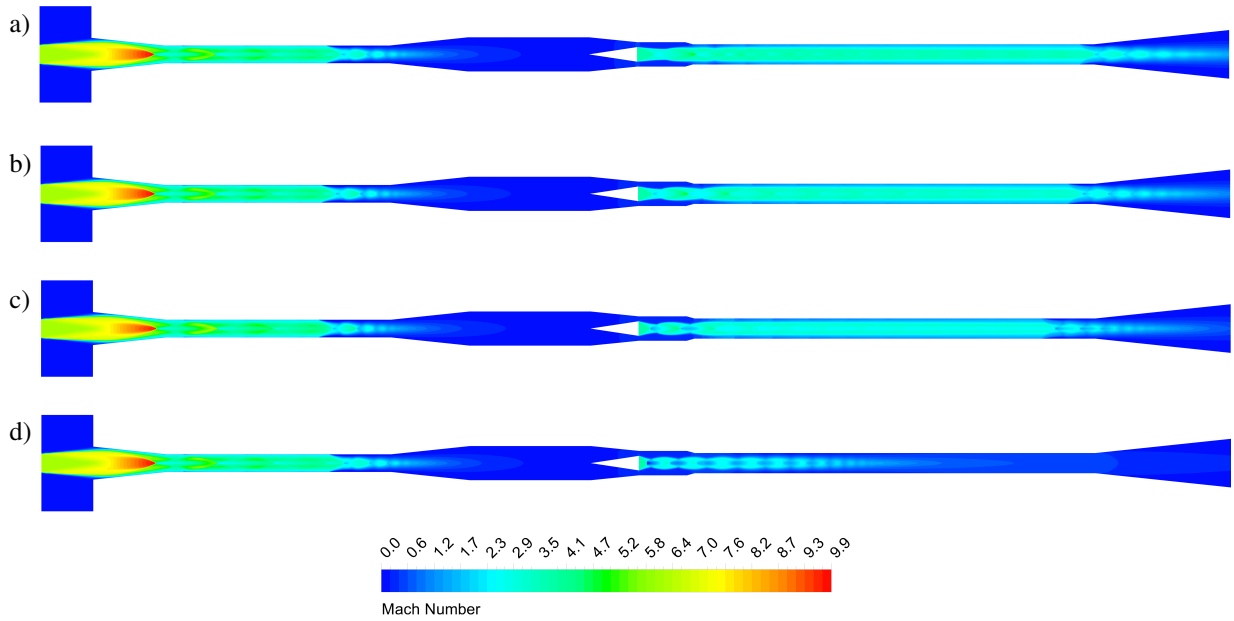

Fig. 9 Computed Mach number contours for the H3 diffuser-ejector system for $P_{0,ej}$ of 25 (a), 20 (b), 15 (c) and 10 bar (d)

3. Experimental ejector performance characteristics

Several experiments have been carried out in order to assess the ejector characteristic for zero secondary mass flow rate (i.e. facility valve closed) and hence find the transition point that corresponds to the optimum ejector operation: it gives the lowest possible pressure in the test chamber with the minimum ejector total pressure [31]. Typical results are showed in Fig. 10(a), in which we present the effect of a step-by-step change of the ejector total pressure $P_{0,ej}$ on the test chamber pressure. No major influence is visible on the test chamber pressure for $P_{0,ej}$ higher than 15 bar: the supersonic flow regime is achieved in this case. It is important to notice that, before reaching the stable supersonic regime, a locomotive noise, noticed also by Kordulla in [7], can be heard, which corresponds to oscillations in the test chamber pressure. In these conditions indeed, the ejector total pressure is still not high enough to let the shocks train be stable in the ejector diffuser throat and makes them oscillate. As the shocks oscillate in the ejector diffuser, the flow conditions at the ejector diffuser exit change from supersonic to subsonic creating the characteristic locomotive noise: the frequency of the noise is therefore the frequency of oscillation of the shocks inside the ejector diffuser throat.

The correspondence between this oscillation phenomenon and the transition point can be seen in Fig. 10(b), in which we present the ejector performance characteristic with zero secondary mass flow (i.e. facility valve closed). Moreover, it is apparent how the pressure ratio needed to run the ejector is lower than that needed to start it, as it happens in supersonic diffusers [4]: in fact, when increasing $P_{0,ej}$, it is needed a pressure of around 15 bar to reach the supersonic flow regime (i.e. to start the ejector diffuser and therefore to have the shock trains in the ejector diffuser throat) while, when decreasing it, the supersonic regime is stable until a pressure of around 13.5 bar, below which the oscillation phenomena start to be present.

4. Blockage experimental investigation

The operation of a hypersonic diffuser has been shown to be heavily influenced by models' shape, dimensions and position [10, 17–19]. This issue has been underlined in the H3 hypersonic wind tunnel operation during a recent test campaign [3]. It turned out that the main diffuser cannot assure under-expanded conditions for big models due to too large pressure losses (Fig. 11(a)) while, reducing the model dimensions, the flow is brought to a working stable condition (Fig. 11(b)). The stable flow condition has showed to be very sensitive to model position, support shape and sting length.

In order to consider all these parameters, 4 models have been used which differ in terms of shape and dimensions and, for each of them, several tests with varying total flow conditions have been performed (Tab. 1). Moreover, during

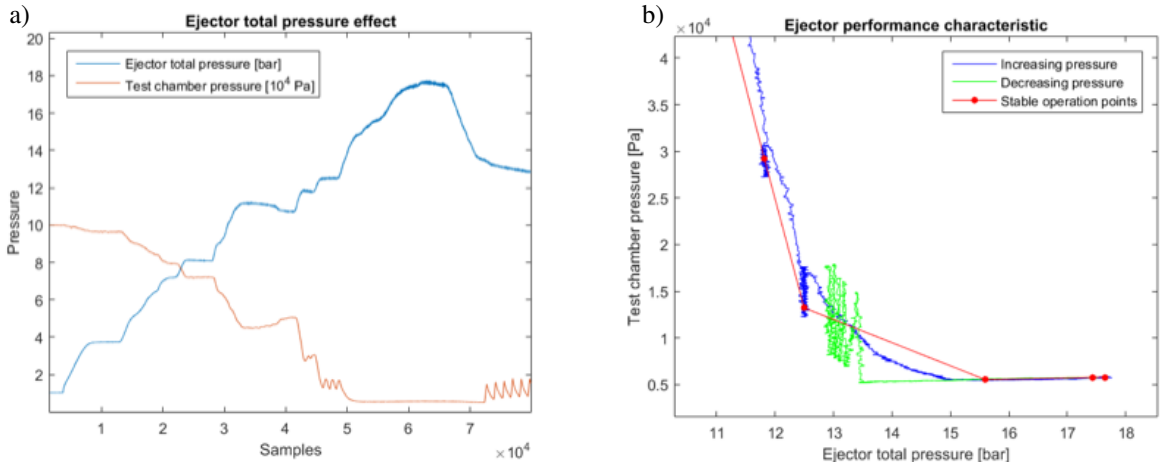

Fig. 10 Investigation of ejector operation with increasing primary total pressure (a) and ejector characteristic with zero secondary mass flow (b)

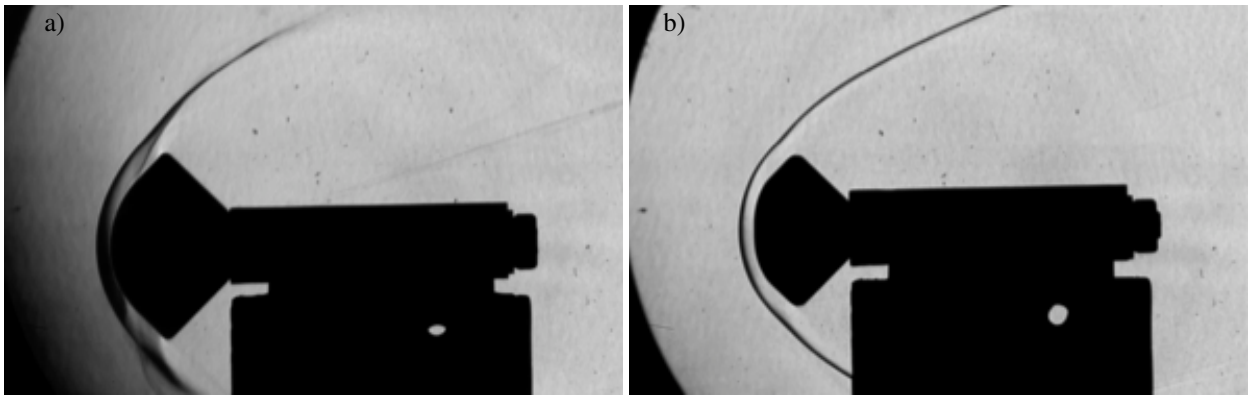

Fig. 11 Schlieren pictures of the unstable shock in front of the Phoebus model of 5 cm during injection (a) and stable shock in front of the Phoebus model of 4 cm during wind tunnel run (b)

each test, the model was moved in the test chamber: the starting model position was close to the diffuser catch cone and it was moved upstream reaching almost the nozzle exit position. At this point the direction of movement was reversed and the model went back to almost the same starting position. To limit the effect of the sting length, it has been chosen to be equal to the model length in the flow direction.

With the small and the medium blunt models, the tunnel was correctly operated in all operating conditions. This was not the case with the large blunt model that did not allow to establish a stable supersonic flow in the test chamber, being too big for the H3 wind tunnel testing capabilities. Typical results of the experimental investigation are showed in Fig. 12 for the small blunt model. It is apparent that when the model moves toward the nozzle, the test chamber pressure increases considerably meaning that the total pressure losses are higher, and that the diffuser efficiency is lower. Indeed, the closer is the model to the catch cone, the better the diffuser is able to catch the flow deviated by the model, recover pressure and maintain a low pressure in the test chamber. What therefore matters is not the distance between the nozzle exit and the model in se, but the distance between the model and the diffuser catch cone which should be minimized. A small hysteresis is also present in the measurements: when the direction of the model is inverted, the test chamber pressure does not go back to the same values but the “moving model downstream” curve shows higher pressure losses than the “moving model upstream” one. This is due the difficulty of the diffuser in discharging the pressure accumulated in the test chamber once a high value has been achieved, as in [10]. The large change in diffuser operation is apparent also from the plot of the diffuser efficiency (defined as in [26]) as a function of the model position in the test chamber (Fig. 12(b)).

A very interesting test has been carried out on the medium blunt model at 10 bar in which the model injection could

Table 1 Wind tunnel models used in the blockage investigation

Model	Shape	Dimensions [mm]	Blockage ratio [%]
Pitot rake	Ramp 24 degrees with tubes	120 x 12	8.8 + side tubes
Small blunt model	Bullet	25 max. diameter	3
Medium blunt model	Phoebus capsule	40 max. diameter	7.7
Large blunt model	Phoebus capsule	50 max. diameter	12

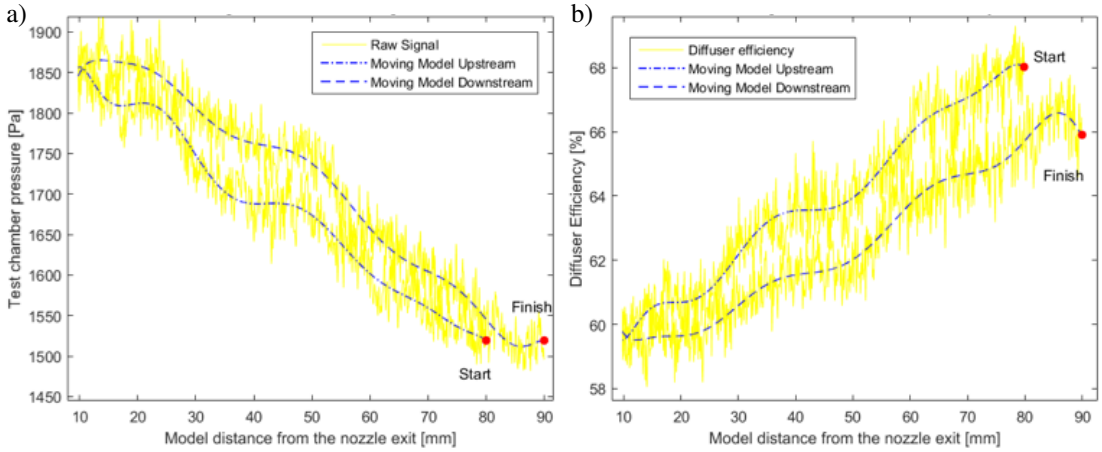

Fig. 12 Test chamber pressure (a) and diffuser efficiency (b) with moving model (small blunt model, 25 bar)

be performed correctly but, while the model was moving upstream, at around 40 mm from the nozzle, the blockage of the diffuser has been observed with the upstream movement of the shock train to the test chamber. The medium blunt model (i.e. 7.7 % of blockage ratio) seems therefore to be the limit for the current H3 testing capabilities. Diffuser efficiency as a function of the total pressure and Reynolds number for different models is presented Fig. 13. For each type of model, as it happens for the empty test section, the average diffuser efficiency is an increasing function of the Reynolds number and, hence, of the total pressure (at fixed T_0), confirming the trend found by Boylan [10].

IV. Experimental campaign on low-temperature ablators

A. Low temperature ablative models

Wind tunnel characterization is of fundamental importance for carrying out experiments with low uncertainty on flow conditions and wind tunnel operation. In hypersonic wind tunnels it is possible for example to study the ablation process linked to the need to develop suitable protection systems (TPS) for vehicles that undergo planetary entry. However, use of real TPS materials is usually difficult because of too many phenomena involved in the ablation process and high operational cost of plasma wind tunnels. Low temperature ablative materials instead can be easily used in cold hypersonic wind tunnels to study simplified ablation process. These materials are characterized by a high vapor pressure at ambient conditions, which turns into sublimation when injected in a high temperature flow with low static pressure [36–40, 40, 41]. Fundamental in the aerothermodynamics studies that regard the interaction between the ablation process and the boundary layer is to have a good surface quality of the models and good mechanical properties in order to withstand the high dynamic pressure without major issues on the model integrity. The solution to these requirements has been found in the sintering process of models starting from vacuumed naphthalene and camphor powders [37–39]. Based on these works, a sintering machine has been designed and built at the VKI Workshop: typical test results in the H3 wind tunnel are shown in Fig. 14, showing good surface quality and mechanical properties of the models (i.e. the surface is not just swept away by the flow). In this test, a black and white pattern has been projected in the test chamber since recognizable features on the model surface are required for the ablation rate measurement [3]. The ablation process is clearly visible with a change in the model shape (a-c) and when the thickness of the camphor

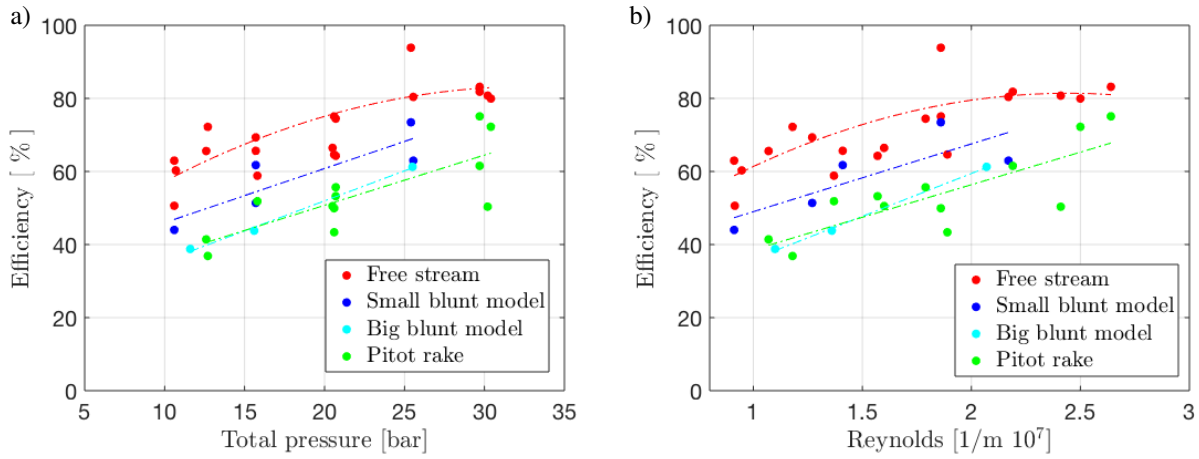

Fig. 13 Experimental H3 diffuser efficiency for different models as a function of the total pressure (a) and of the Reynolds number (b)

part is strongly reduced, a fracture in the solid is visible (c). Toward the end of the experiment, it can be seen how only the front part of the model has been completely eroded since it has been exposed to higher heat flux. The outer portion of the bow shock may be observed in the upper part of the flow field (underneath the blue dots in Fig. 14(a) thanks to the light deflection caused by the refractive index gradient. Looking at Figures Fig. 14(b-d) it is possible to see how the shock changes shape and position according to the different shape of the model undergoing the ablation process.

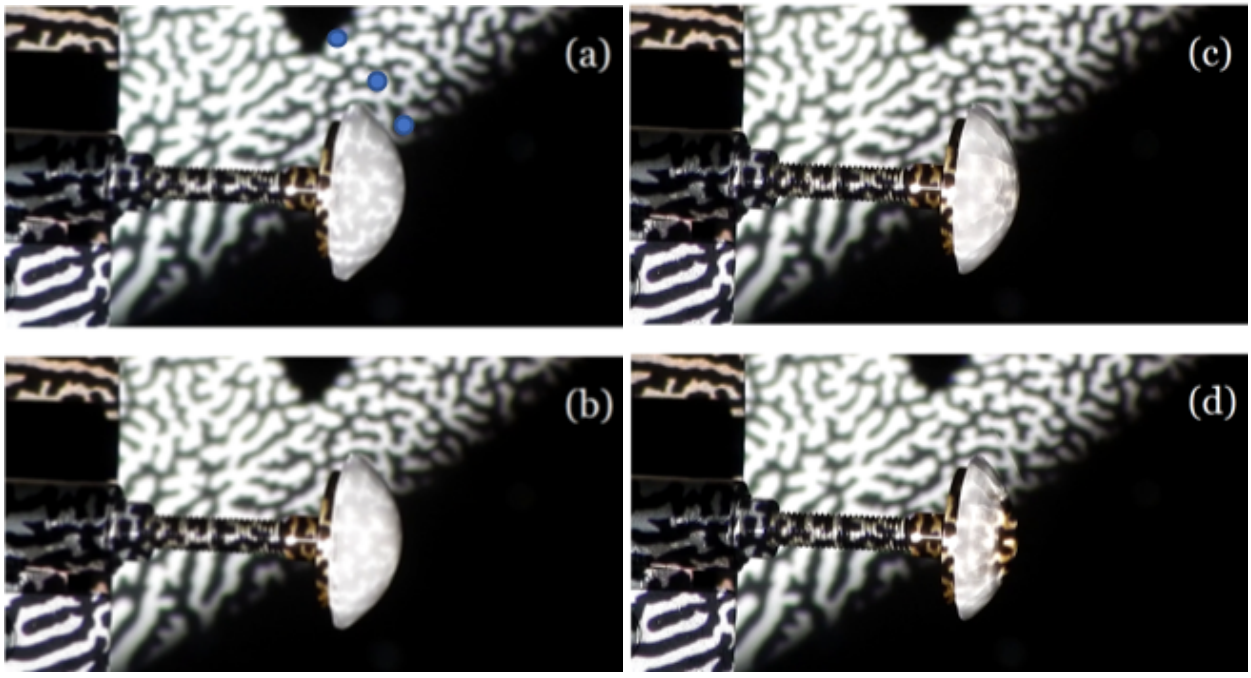

Fig. 14 Testing the sintered Phoebus model, the bow shock is visible

B. PLIF tool

The recent interest in using naphthalene as low temperature ablative material is due to its fluorescence properties, for which PLIF (i.e. planar laser induced fluorescence) technique can be applied for flow visualization. Naphthalene can be electronically excited by using a light with 266 nm of wavelength giving back the energy absorbed as a fluorescence

signal [36]. The intensity of the fluorescence signal is proportional to the molar fraction of naphthalene, but it is also strongly affected by the presence of other molecules, which effect causes excited molecules to return directly to the ground state via non-radiative process, called quenching. The knowledge of the quenching cross section of different species is of fundamental importance to calculate the time-integrated fluorescence signal S_f, showed in Eq. 3 in units of photons [36].

$$S_f = \frac{E}{hc/\lambda}\eta\Delta V\chi_i n(P,T)\sigma_a(\lambda,T)\phi(\lambda,P,T,\chi) \tag{3}$$

In the above equation, E is the laser fluence (J/m2), h is the Planck's constant, c is the speed of light, λ is the wavelength of the laser, η is the optics collection efficiency, ΔV the is the volume of molecules interested by the laser light; χ_i is the species mole fraction, n is the total number density, σ_a is the absorption cross section, ϕ is the fluorescence yield in which there is the quenching cross section and finally P and T are pressure and temperature. From Eq. 3 it is possible to calculate the mole fraction and therefore the density of naphthalene, adopting the approach suggested by many recent studies, e.g. [36]. However, in the present investigation, no attempts have been made to perform quantitative measurements of ablation-products transport. A detailed qualitative study on the possibility of using PLIF for flow visualization in the H3 wind tunnel has instead been successfully performed.

C. Setup description

The PLIF setup is composed by the excitation module which contains the laser and a system of lenses to provide a laser sheet at 266 nm, and by the detection module that contains the camera linked to a computer with some filters for rejecting external disturbances.

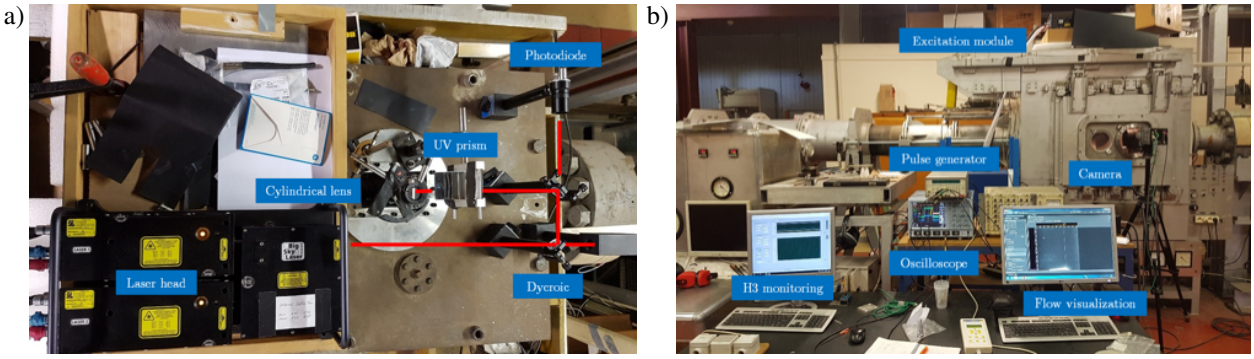

Fig. 15 Setup for the PLIF measurements, the excitation module is on the top of the test chamber (a) while the detection module is near it (b)

In particular, the laser head has been installed on the top of the test chamber providing a laser sheet from the top of it on the model, and, in order to reduce the facility vibrations, a box filled with sand has been used as support for the laser system (Fig. 15(a)). The detection module is installed at the side of the test chamber where the proper optical window transparent to UV radiation has been installed (Fig. 15(b)). The excitation module is based on a pulsed Nd:YAG solid-state laser (Quantel Big Sky Laser) operating up to 15 Hz. A second harmonic generation is combined with a wavelength separation assembly to produce 200 mJ laser pulse at 532 nm, while UV radiation at 266 nm is generated through thermally controlled non-linear crystal with relevant separation optics. The detection module is based on an ICCD camera (PI-MAX 3) with a Sodern Cerco UV lens that collects the fluorescent signal and it is combined with adequate filters to eliminate noisy background. PLIF signal is acquired using 0.5 μs camera gate and a constant gain of 45. In order to improve signal-to-noise ratio ICCD binning has been carried out, with a corresponding detection system spatial resolution of 770 μm. The synchronization system provided by a Stanford DG535 digital delay/pulse generator controls the laser energy, releases the laser pulse and opens the camera lens at the right moment (i.e. fluorescence lifetime is in the order of 10 ns).

D. Test campaign results

Experiments have been carried out on a re-entry capsule bullet shape model made by naphthalene with the same dimensions of the small blunt model used in our blockage investigation (Fig. 16).

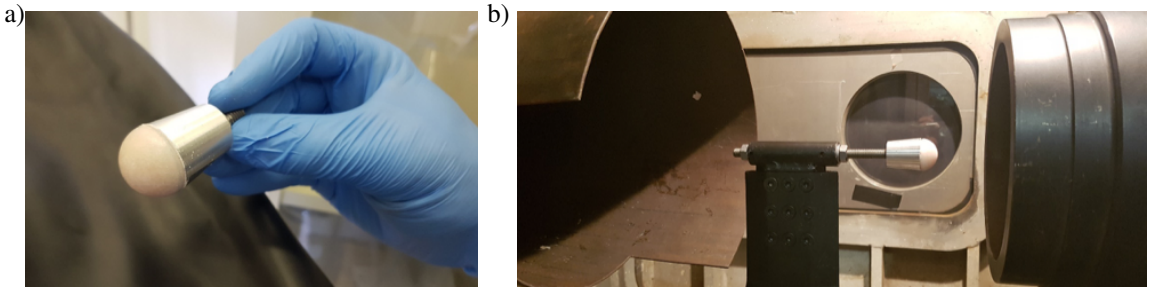

Fig. 16 Naphthalene test capsule for the PLIF experiment details (a) and at 0° angle of attack in the test chamber (b)

Figure 17 shows the post-processed PLIF images of the capsule model at 0° angle of attack (P_0 of 20 bar and T_0 of 530 K), where the fluorescence signal has been normalized in each frame with respect to the maximum. The ablation process is clearly visible: in around 25 seconds from image a to h, the naphthalene heat shield is completely eroded. In image a, when the model is just injected, we can only see the starting solid shape of the capsule, since no major ablation is happening, and the naphthalene vapor is not present yet. After a few moments, the ablation process starts (b) and a laminar naphthalene vapor phase is present on the model and in the back region. As soon as the temperature of the model increases, at around 7 seconds after the model injection, the capsule starts to deform (c) with some liquid melt naphthalene being recrystallized near the model metallic part. From this point on, the flow on the model and in the back region is clearly turbulent and unsteady (d-g): we are observing a laminar-turbulent transition due to ablation process. In practice the changing shape of the capsule and the increasing roughness of the surface together with the blowing of naphthalene vapor trig the laminar-turbulent transition. In fact, it is well known that blowing generally moves transition upstream, with larger mass flow rates (i.e. larger ablation) causing a larger eect [42]. Finally, after approximately 22 s (h), the initial shape is no longer recognizable, and less naphthalene vapor is being transported due to the less solid present on the capsule.

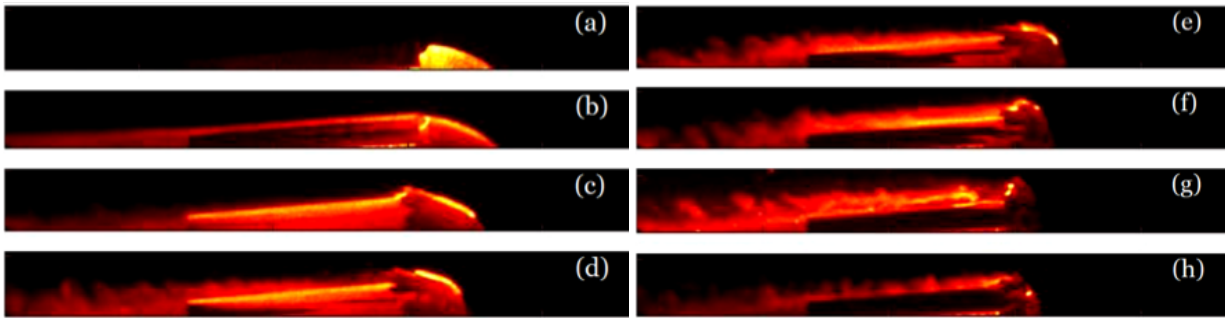

Fig. 17 Naphthalene PLIF images of a capsule model at 0° angle of attack. Images were collected during one run and images a-h are sequential in time from the injection to the ejection of the model

The laminar-turbulent transition is apparent from Fig. 18 where colored contours show the variation about the mean value that is an indication of the turbulence level of the flow. If in the first few seconds, the flow is quite laminar in the back part of the model, with small fluctuation about the mean, it becomes strongly turbulent after around 7 seconds. In the second image we can see that the flow is turbulent from the end of the naphthalene shield. It is possible to see that several vortices separate from the model surface end. The last image shows how the naphthalene capsule has been deformed and, in addition to the turbulent boundary layer, a turbulent wake is leaving the model. The present results demonstrate the capability of the PLIF tool to visualize the flow structures on a low temperature ablative model: laminar-turbulent transition and vortices structures can be detected and analyzed giving important information on the

interaction between ablation process and boundary layer.

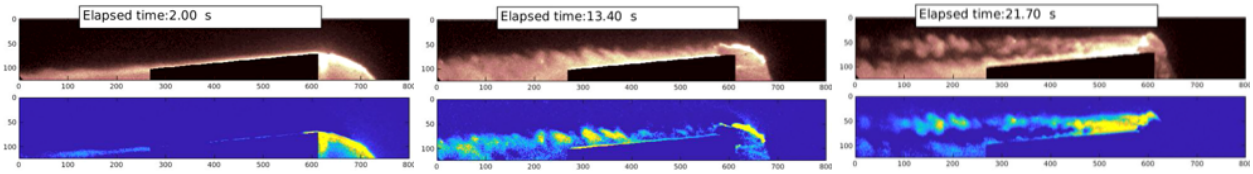

Fig. 18 Naphthalene fluorescence signal (above) and fluctuations about the mean (below) for a capsule model at 0° angle of attack

Conclusion

A detailed benchmark for the evaluation of hypersonic wind tunnels testing capabilities has been presented and applied for the complete characterization of the H3 hypersonic wind tunnel at the von Karman Institute for Fluid Dynamics. The quality of the flow in the test chamber has been checked by performing a calibration with a pitot rake for the whole H3 operating envelope showing uniform flow evolution. Furthermore, an analysis of the diffuser-ejector system in free stream conditions and with models in the test chamber has been conducted both via CFD analyses and with experimental test campaign. CFD analyses of the diffuser-ejector system, validated by experimental data, show that the diffuser efficiency is satisfactory and that the ejector optimum operation is achieved for an ejector total pressure around 15 bar. Investigating blockage effects, with models of different dimensions, has allowed to determine the maximum dimensions of a blunt model that can be tested in the whole operating envelope in the H3 facility and to assess the important role played by the model position along the chamber axis. Finally, the H3 WT has been employed to the study of low temperature ablative models. A sintering machine has been properly designed in order to build naphthalene models and the Planar Laser-Induced Fluorescence tool has been used to qualitatively study the ablation process and its interaction with the boundary layer. In particular, the laminar-turbulent transition due to the ablation process has been observed together with the presence of unsteady structures in the backflow region.

References

[1] Anderson Jr, J. D., *Hypersonic and high-temperature gas dynamics*, American Institute of Aeronautics and Astronautics, 2006.

[2] Simeonides, G., "The VKI hypersonic wind tunnels and associated measurement techniques," Tech. rep., Von Karman Institute for Fluid Dynamics, 1990.

[3] Turchi, A., "Modelling Capsule Stability Accounting for Shape Change. Technical, Implementation, Management and Financial Proposal," Tech. rep., Von Karman Institute for Fluid Dynamics, 2017.

[4] Pope, A., and Goin, K., "High-speed Wind Tunnel Testing," , 1978.

[5] Kammeyer, M., "Wind tunnel facility calibrations and experimental uncertainty," *20th AIAA Advanced Measurement and Ground Testing Technology Conference*, 1998, p. 2715.

[6] Masutti, D., "Ground testing investigation of hypersonic transition phenomena for a re-entry vehicle," 2013.

[7] Kordulla, W., "Calibration of the hypersonic blowdown wind tunnel H-3," Tech. rep., Von Karman Institute for Fluid Dynamics, 1970.

[8] Vanhée, J. L., "The H-3 hypersonic wind tunnel: new implementation and calibration," Tech. rep., Von Karman Institute for Fluid Dynamics, 1989.

[9] Boerrigter, H. L., "Calibration of the H3 Wind Tunnel using Pitot Probes," Tech. rep., Von Karman Institute for Fluid Dynamics, 1993.

[10] Boylan, D. E., "An Experimental Study of Diffusers in an Openjet, Low-Density, Hypersonic Wind Tunnel," Tech. rep., Arnold Engineering Development Center Arnold AFB TN, 1964.

[11] Van Hove, B., "Free stream measurements and a new data reduction method for the VKI Longshot hypersonic wind tunnel," Tech. rep., Von Karman Institute for Fluid Dynamics, 2010.

[12] Korkegi, R., "Experimental facilities at TCEA," Tech. rep., Von Karman Institute for Fluid Dynamics, 1961.

[13] DeLoach, R., "Applications of modern experiment design to wind tunnel testing at NASA Langley Research Center," *36th AIAA Aerospace Sciences Meeting and Exhibit*, 1998, p. 713.

[14] Rhode, M., and DeLoach, R., "Hypersonic wind tunnel calibration using the modern design of experiments," *41st AIAA/ASME/SAE/ASEE Joint Propulsion Conference & Exhibit*, 2005, p. 4274.

[15] Harris, W. G., and McCormick, R. B., "Diffuser Investigation in an Axisymmetric Open Jet, Hypersonic Wind Tunnel," *PREPRINT of a paper presented by Boeing Aircraft Company, Seattle, Washington at AGARD-Sta Meeting*, 1959.

[16] Monnerie, B., "Etude d'une famille de diffuseurs pour soufflerie hypersonique a faible nombre de Reynolds," *Extrait de: La Recherche Aerospatiale*, , No. 114, 1966.

[17] Austin, R. F., "An Open-Jet Wind Tunnel Investigation of a Fixed-Geometry Diffuser System at Mach Numbers 3.6 and 7.0," Tech. rep., Arnold Engineering Development Center Arnold AFB TN, 1966.

[18] White III, J. J., "An Experimental Investigation of Fixed-Geometry Diffusers in an Open-Jet Wind Tunnel at Mach Numbers Between 14 and 18 and Reynolds Numbers Between 8,900 and 25,000," Tech. rep., Arnold Engineering Development Center Arnold AFS TN, 1967.

[19] HANUS, G., MIKKELSEN, K., OLSTAD, S., and Caristia, S., "Supersonic wind tunnel diffuser performance with high model blockageat moderate to low Reynolds numbers," *27th Joint Propulsion Conference*, 1991, p. 2274.

[20] Lukasiewicz, J., "Diffusers for supersonic wind tunnels," *Journal of the aeronautical sciences*, Vol. 20, No. 9, 1953, pp. 617–626.

[21] Waltrup, P., and Billig, F., "Structure of shock waves in cylindrical ducts," *AIAA journal*, Vol. 11, No. 10, 1973, pp. 1404–1408.

[22] Savino, R., Monti, R., and Esposito, A., "Behaviour of hypersonic wind tunnels diffusers at low Reynolds numbers," *Aerospace science and technology*, Vol. 3, No. 1, 1999, pp. 11–19.

[23] Monti, R., Paterna, D., Savino, R., and Esposito, A., "Low-Reynolds number supersonic diffuser for a plasma-heated wind tunnel," *International journal of thermal sciences*, Vol. 40, No. 9, 2001, pp. 804–815.

[24] Pugazenthi, R., and McIntosh, A. C., "Design and performance analysis of a supersonic diffuser for plasma wing tunnel," *International Journal of Aerospace and Mechanical Engineering*, Vol. 5, No. 8, 2011, pp. 1682–1687.

[25] Sparrow, E., Abraham, J., and Minkowycz, W., "Flow separation in a diverging conical duct: Effect of Reynolds number and divergence angle," *International Journal of Heat and Mass Transfer*, Vol. 52, No. 13-14, 2009, pp. 3079–3083.

[26] Hermann, R., "Diffuser efficiency and flow process of supersonic wind tunnels with free jet test section," Tech. rep., Air Materiel Command Wright-Patterson AFB OH, 1950.

[27] Purpura, C., De Filippis, F., Barrera, P., and Mandanici, D., "Experimental characterisation of the CIRA plasma wind tunnel SCIROCCO test section," *Acta Astronautica*, Vol. 62, No. 6-7, 2008, pp. 410–421.

[28] Rao, S., and Jagadeesha, G., "Aerodynamic Design of Supersonic Ejectors for Wind Tunnel Applications," *National Conference on Wind Tunnel Testing*, Vol. 2, ????, p. 6.

[29] Uelbelhack, H., "Supersonic ejector with second throat diffusers," Tech. rep., Von Karman Institute for Fluid Dynamics, 1965.

[30] Ginoux, J. J., "Supersonic Ejectors." Tech. rep., ADVISORY GROUP FOR AEROSPACE RESEARCH AND DEVELOPMENT PARIS (FRANCE), 1972.

[31] Fabri, J., and Paulon, J., "Theory and Experiments on Supersonic Air-to-Air Ejectors." 1958.

[32] Agostinelli, P. W., Trifoni, E., and Savino, R., "Aerothermodynamic analyses and redesign of GHIBLI Plasma Wind Tunnel hypersonic diffuser," *Aerospace Science and Technology*, Vol. 87, 2019, pp. 218–229.

[33] Liou, M.-S., and Steffen Jr, C. J., "A new flux splitting scheme," *Journal of Computational physics*, Vol. 107, No. 1, 1993, pp. 23–39.

[34] Menter, F., "Zonal two equation kw turbulence models for aerodynamic flows," *23rd fluid dynamics, plasmadynamics, and lasers conference*, 1993, p. 2906.

[35] Scoggins, J. B., and Magin, T. E., "Development of mutation++: Multicomponent thermodynamic and transport properties for ionized plasmas written in c++," *11th AIAA/ASME joint thermophysics and heat transfer conference*, 2014, p. 2966.

[36] Combs, C. S., et al., "Quantitative measurements of ablation-products transport in supersonic turbulent flows using planar laser-induced fluorescence," Ph.D. thesis, 2015.

[37] Charwat, A. F., "Exploratory studies on the sublimation of slender camphor and naphthalene models in a supersonic wind-tunnel," Tech. rep., RAND CORP SANTA MONICA CA, 1968.

[38] Stock, H. W., and Ginoux, J. J., "Hypersonic Low Temperature Ablation an Experimental Study of Cross-Hatched Surface Patterns," *Astronautical Research 1971*, Springer, 1973, pp. 105–120.

[39] Stock, H. W., and Ginoux, J. J., "Hypersonic Low Temperature Ablation an Experimental Study of Cross-Hatched Surface Patterns," *Astronautical Research 1971*, Springer, 1973, pp. 105–120.

[40] Stock, H. W., and Ginoux, J. J., "Experimental results on crosshatched ablation patterns," *AIAA Journal*, Vol. 9, No. 5, 1971, pp. 971–973.

[41] Combs, C., Clemens, N. T., and Danehy, P. M., "Development of naphthalene PLIF for visualizing ablation products from a space capsule heat shield," *52nd Aerospace Sciences Meeting*, 2014, p. 1152.

[42] Schneider, S. P., "Hypersonic boundary-layer transition with ablation and blowing," *Journal of Spacecraft and Rockets*, Vol. 47, No. 2, 2010, pp. 225–237.